Journal of Power Sources 265 (2014) 356–362

Contents lists available at ScienceDirect

Journal of Power Sources

journal homepage: www.elsevier.com/locate/jpowsour

Failure analysis of pinch–torsion tests as a thermal runaway risk evaluation method of Li-ion cells

Yuzhi Xia [a], Tianlei Li [b], Fei Ren [c], Yanfei Gao [a,d], Hsin Wang [d,*]

[a] Department of Materials Science and Engineering, University of Tennessee, Knoxville, TN 37996, USA
[b] National High Magnetic Field Laboratory, Florida State University, Tallahassee, FL 32310, USA
[c] Department of Mechanical Engineering, Temple University, Philadelphia, PA 19122, USA
[d] Materials Science and Technology Division, Oak Ridge National Laboratory, Oak Ridge, TN 37831, USA

HIGHLIGHTS

- Finite element models are developed to evaluate the effectiveness of the pinch–torsion test in creating ISCrs in Li-ion cell.
- The torsion component can trigger ISCr at a lower load with smaller short spot size.
- This method can distinguish commercial cell safety performance in their entire range of SOC.

ARTICLE INFO

Article history:
Received 17 February 2014
Received in revised form
9 April 2014
Accepted 10 April 2014
Available online 25 April 2014

Keywords:
Li-ion battery
Finite element analysis
Pinch–torsion test
Fracture
Internal short circuit

ABSTRACT

Recently a pinch–torsion test is developed for safety testing of Li-ion batteries. It has been demonstrated that this test can generate small internal short-circuit spots in the separator in a controllable and repeatable manner. In the current research, the failure mechanism is examined by numerical simulations and comparisons to experimental observations. Finite element models are developed to evaluate the deformation of the separators under both pure pinch and pinch–torsion loading conditions. It is discovered that the addition of the torsion component significantly increased the maximum first principal strain, which is believed to induce the internal short circuit. In addition, the applied load in the pinch–torsion test is significantly less than in the pure pinch test, thus dramatically improving the applicability of this method to ultra-thick batteries which otherwise require heavy load in excess of machine capability. It is further found that the separator failure is achieved in the early stage of torsion (within a few degree of rotation). Effect of coefficient of friction on the maximum first principal strain is also examined.

1. Introduction

Lithium-ion batteries are becoming a primary power source in our daily lives through electronic devices (cell phones, tablets and laptops) and transportations (hybrid and electric vehicles, and airplanes). These applications are demanding more power output, higher power density and lower cost, sometimes at the expense of safety. Safety hazard related issues of Li-ion cells have been well documented [1,2]. Many major field incidents are caused by externally or internally (e.g., manufacturing defects, mechanical abuse, usage abuse, etc.) induced short circuits, which can potentially release the high energy stored in the battery in very short time locally and trigger chemical chain reactions releasing a massive amount of heat. If the battery is not well designed such that the heat cannot be conducted away quickly, thermal runaway could happen and lead to fires and explosions in some extreme cases [3,4]. Among these safety concerns, internal short circuit (ISCr) under no obvious abuse or external triggers are less understood and very difficult to reproduce experimentally. Therefore, evaluating the thermal runaway risk of Li-ion batteries by experimentally creating ISCr in a controllable and predictable manner has brought broad interests to the field.

In order to evaluate the risk of thermal runaway, many tests have been conducted to simulate ISCr event via internal defect initiation, including forced ISCr test by the Battery Association of Japan [5], instrumented indentation [6,7] and nail penetration [8].

* Corresponding author. Tel.: +1 865 576 5074.
E-mail address: wangh2@ornl.gov (H. Wang).

http://dx.doi.org/10.1016/j.jpowsour.2014.04.040
0378-7753/

Nomenclature

a	contact radius
$c(\theta)$	distance between the maximum tangential traction location and the contact center
F_0	the applied load on the indenter in pinch only test
h	the thickness of cathode, separator, and anode layers in the unit cell
ISCr	internal short circuit
M_z	the twist moment applied on the indenter
$p(r)$	normal contact pressure distribution in the contact area
$q(r)$	tangential traction in the contact area
r	distance to the contact center in the contact area
u_1, u_2, u_3	displacements respectively in x, y, z direction in Fig. 2
u_4, u_5, u_6	rotations respectively along x, y, z direction in Fig. 2
ε_0	the maximum first principle strain in pinch only test with the load F_0
ε_I	the first principal strain
$\varepsilon_{I_{max}}$	the maximum first principal strain
ε_{III}	the third principal strain
ε_Y	yield strain
θ	twist angle
μ	friction coefficient
σ_Y	yield strength
σ_u	ultimate strength

We recently reported an improved pinch test method [9,10] that could reproducibly create controllable ISCr in a cell separator where the size of the ISCr spots depends on the loading speed, pinch ball or indenter diameter, and stroke return-voltage. A further development of this pinch test method added a torsional loading component, which exhibited improvement in the effectiveness of creating the ISCr [11]. It was demonstrated in two different commercial Li-ion cells that the torsion facilitated the occurrence of ISCr with lower axial load and smaller ISCr spot size. This method is thus potentially applicable to very thick batteries, for which the critical loads under pure pinch tests are too large for the standard loading apparatus.

In order to quantitatively relate the pinch–torsion tests to the thermal runaway failure in batteries, it is of critical importance to understand the deformation and failure mechanisms under such loading conditions. For instance, what is the dependence of the critical normal/twist load on the indenter radius, battery thickness, number of electrode/separator layers, and indenter/battery friction condition, among many other factors? Imagine an application of successive pinch and torsion loads, and one can design the loading pattern/history to conveniently identify the failure initiation and optimize the load magnitude to allow a portable evaluation. Motivated by the above considerations, the present paper attempts to develop a computational model for both test methods (pinch-only and pinch–torsion test systems) and make a systematic investigation on the deformation mechanisms to provide insight for the battery safety assessment. In this paper, finite element method (FEM) is used to simulate the strain field and to predict the defect initiation, which was then compared with experiment results. The effect of surface condition was also discussed to optimize the test design. Moreover, the deformation mechanisms were rationalized by an analytical stick-slip model when both contact and torsion were applied.

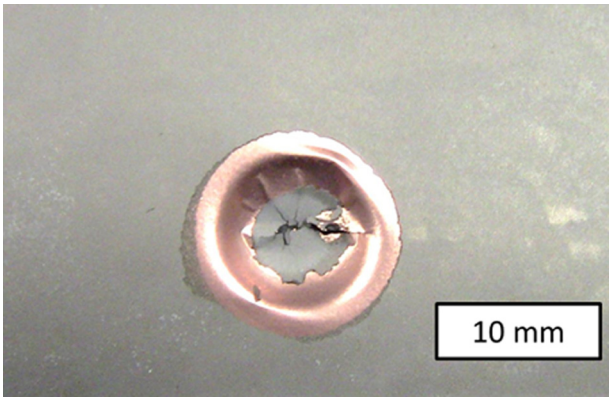

Fig. 1. Optical graph of an anode layer after pinch testing showing most of the graphite coating in the indented region was removed during the test (the gray zone is graphite coating).

2. Numerical model

The repeating functional unit of a dry Li-ion cell contains an anode layer, a cathode layer, and a separator layer. Since electrolytes used in most Li-ion cells are in liquid phase, they are not included in the finite element models. In addition, the active coatings (graphite and lithium salts) are generally loosely bonded powders on the electrodes. During slow pinch–torsion tests, the coating materials were delaminated, worn into small pieces and displaced from the highly stressed zone near the indenter tip. In fact, our experimental observation revealed that the active coating materials were pushed away from the contact area after testing (Fig. 1). Therefore, the coatings structurally bear little load especially comparing with the other components and will be simply excluded in our model. The stress equilibrium equation is $\partial\sigma_{ij}/\partial x_i + b_j = 0$ in which b_j is the body force and is ignored in our model. The strain ε_{ij} are the first derivative of the displacement i.e. $\varepsilon_{ij} = \frac{1}{2}(\partial u_i/\partial x_j + \partial u_j/\partial x_i)$ [13] and stress–strain relationship is given by the constitutive laws which will be discussed later. The boundary value problem is then resolved with commercial finite element package ABAQUS (3DS SIMULIA).

Fig. 2 depicts a three-layer (anode–separator–cathode) unit cell model in the FEM simulation in this study. The material of the top anode layer is Cu, the separator layer in the middle is high-density polyethylene (HDPE) and the bottom cathode layer is Al. The thickness of each layer h is 0.02 mm. The two indenters in the pinch and torsion test are modeled as two rigid spheres and the indenter radius is 12.7 mm. The lateral dimension of the unit cell ($\sim$10 mm) is chosen to be ten times larger than the estimated contact radius

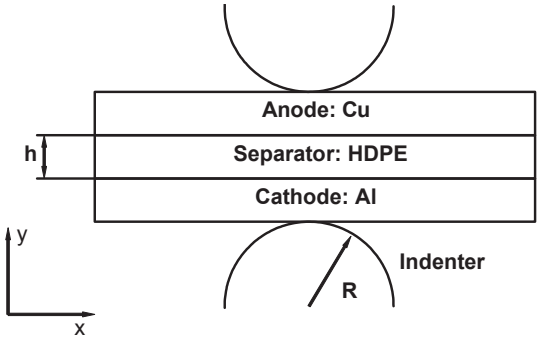

Fig. 2. Schematics of the cross section view of a three-layer battery unit cell system under the pinch tests between two spherical indenters.

Table 1
Material properties of Al and Cu foils measured from uniaxial tension tests [12].

	Aluminum foil	Copper foil
Yield stress, σ_Y (MPa)	180	210
Ultimate stress, σ_u (MPa)	195	230
Yield strain, ε_Y	0.017	0.022
Elongation (%)	2.7	3.5

size (~1 mm) to eliminate the boundary effects. The bottom indenter is fixed (i.e., $u_i = 0$, $i = 1, 2 \ldots 6$). The top indenter is first applied with a translation $u_3 = 0.9h$ vertical to the unit cell top surface and then rotated with displacement boundary condition $u_5 = \theta$ to represent the twisting in the experiment. All other degree of freedoms of the top indenter are zero.

Both Al and Cu materials are modeled as elastic–plastic solids with isotropic hardening laws. Materials parameters used in the finite element model are listed in Table 1. The HDPE material is modeled by the hyperelastic Neo-Hookean material model, where the "strain energy potential" U is based on strain invariants. The form of the Neo-Hookean strain energy potential is

$$U = C_{10}\left(\overline{I_1} - 3\right) + \frac{1}{D_1}\left(J^{el} - 1\right)^2 \quad (1)$$

where $\overline{I_1}$ is the first deviatoric strain invariant and J^{el} is the elastic volume ratio, C_{10} and D_1 are the model parameters determined from the HDPE material stress–strain curve measured from uniaxial tensile test [13]. HDPE materials show various behavior in uniaxial tensile test e.g. monotonic hardening [14] and softening effect where the stress decreases with increasing strain after yield due to the reorientation phenomenon [15]. Representative stress-strain curves of HDPE are shown in Fig. 3. In our analysis, discrete data points from uniaxial tension test are input in the material definition section in ABAQUS.

In order to compare with the experimental procedure and research on the twisting effect to the defect initiation in the HDPE layer, the pinch and torsion tests are modeled in two successive steps in the FEM simulation. In the first step, the top indenter vertically pinches on the top surface of the unit cell. This is an axisymmetric problem and the analysis cost is substantially reduced by using axisymmetric elements compared with a fully three-dimensional model. In this simulation, the displacement of the top indenter is 0.018 mm which is $0.9h$. Large deformation (i.e., geometric nonlinearity) is used in the simulation. In the second twisting step, torsion along z axis is not symmetric with z axis (axis of symmetry in pinch test) and thus $\tau_{z\theta}$ is nonzero in the battery. Therefore a full three-dimensional model is used to simulate the indenter twist in the experiment. The displacement and stress fields result from step one are first imported into the three-dimensional model, and the top indenter is then applied with a maximum rotation angle of 12°. The rigid body motion of the specimen is removed by fixing the transverse translation of the unit cell center line, i.e. $u_i = 0$, $i = 1, 2, 3$. The Coulomb friction model is used between the indenter and the specimen, and the effect of friction coefficient will be studied in details.

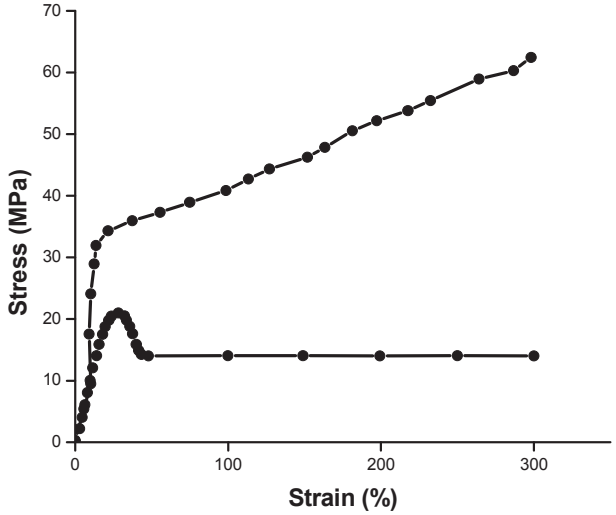

Fig. 3. Representative stress–strain curve of the HDPE material.

Since this paper focus on the initiation of ISCr created by the pinch and torsion tests, the surface interactions within the unit cell are not considered. Therefore, we tie each contact surfaces within the unit cell, i.e. surfaces between the Al and separator layers and surfaces between Cu and separator layers to reduce the computation cost from the contact iterations and numerical divergence in ABAQUS.

3. FEM results and discussion

3.1. Pinch test

In the pinch and torsion experiments [11], ISCr in the Li-ion battery is intentionally created by breaking the separator layer to trigger the chemical reactions. The cell was charged to a set level and the open voltage between the anode and the cathode is closely monitored to ensure that the indenter will be retreated immediately whenever a selected voltage drop (e.g. 0.1 V) is measured. There was no additional charge/discharge occurred during the mechanical test. There is some volume change during charge/discharge, which adds mechanical stress. However, since the current research focus on externally applied mechanical force to induce failure, the electrochemistry induced mechanical behavior is not studied in this paper. The failure of the separator is due to the high tensile strain caused by the contact. To predict the ISCr location, the tensile zone in the separator layer in the unit cell beneath the spherical contact is characterized by the absolute value of the first principal strain over the third principal strain, i.e. $|\varepsilon_I/\varepsilon_{III}|$, and is plotted as a top view in Fig. 4a. Experimental research shows that the ductile failure process in HDPE occurs due to the localized necking after excessive elongation at an intermediate strain rate, a typical rate for our pinch–torsion test [16]. When $|\varepsilon_I/\varepsilon_{III}| > 1$, the location is under tension state where the necking is mostly likely to initiate (denoted as red zones in Fig. 4a). The blue zone in Fig. 4a undergoes compressive deformation. It is shown that the spherical indentation results into a local tension zone in the separator near the indenter but outside the contact area. The inner radius r of the tension zone is about $1.2a$ and the outer radius is approximate $1.8a$ where a is the contact radius. The distribution of the first principal strain ε_I in the separator is shown in Fig. 4b. The highest value of first principal strain ε_I in separator layer exists at the point $1.35a$ away from the center and is under tension. This simulation result qualitatively agrees with our experimental examination such that holes on the separators usually appeared at locations some distance away from the center of the impression as shown in Fig. 5. After pinch (Fig. 5a) and pinch torsion test (Fig. 5b), the separators layer in the unit cell are observed with a hole outside the contact area.

3.2. Pinch–torsion test

It has been observed that some initial axial load needed to create ISCr in the unit cell drops significantly if a small amount of torsion

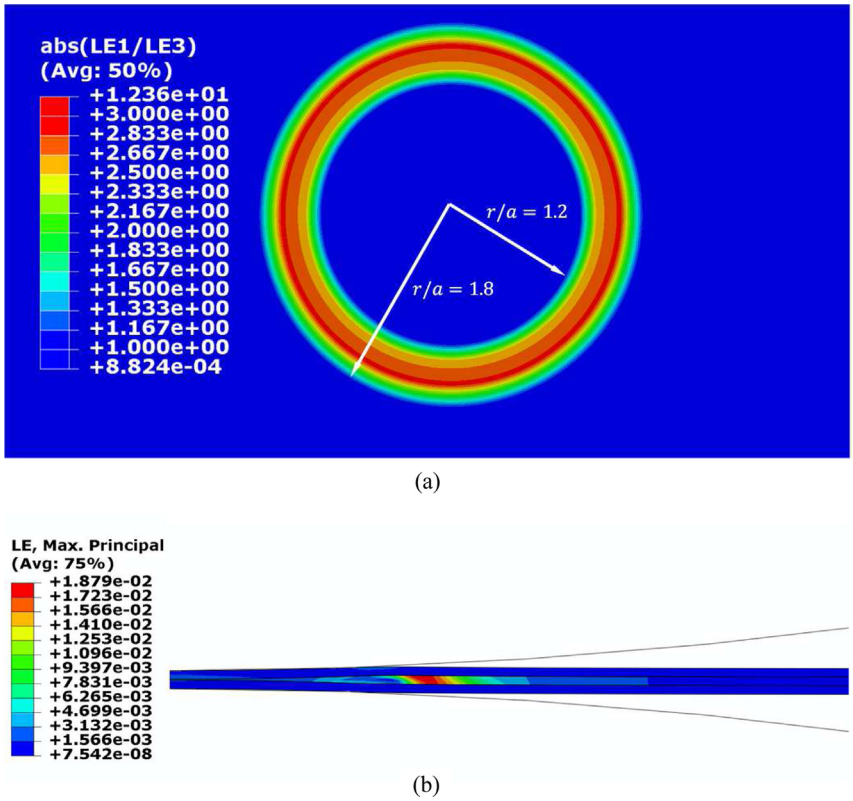

Fig. 4. (a) Top-view contours of absolute value of $\varepsilon_I/\varepsilon_{III}$ in the separator layer in pinch-only test. The non-blue colors denote the region under tension. (b) Cross section view of the distribution of maximum first principal strain ε_I after an indentation of 0.018 mm in unit cell. (For interpretation of the references to color in this figure legend, the reader is referred to the web version of this article.)

is applied on the indenter in our recently developed pinch–torsion test method [11]. To investigate the effect of torsional component on initiating defect during pinch test, a full three-dimensional torsion model is simulated. As stated earlier, we first import data from the pure pinch test and then conduct a static analysis by applying a rotation on the indenter. Fig. 6 shows the comparison of the strain fields in the separator in top view before (Fig. 6a) and after (Fig. 6b) the torsion is applied. The friction coefficients between the indenter and the unit cell top and bottom surfaces are chosen to be 0.3. After the torsion, the size of the tension zone is not changed noticeably. However, the maximum first principal strain ε_I in the tension zone increases significantly (by 77.7%) after the indenter is twisted by 12°. It demonstrates that a slight twisting of the indenter can assist the defect generation which is consistent with our experimental observation [11]. In order to understand the effect of friction coefficient between the contact surfaces, μ, on the pinch and torsion test, the maximum first principal strain ε_I is plotted as a function of θ in Fig. 7 for three different friction coefficient values. When a small twist is applied to the indenter, ε_I increases almost linearly with the twist angle. The slope of ε_I and θ curve gradually decrease with increasing twist angle until ε_I reaches a plateau at a twist angle about 5°.

The above phenomenon can be explained by an elastic contact analysis [17–19]. For an elastic half-space under spherical contact, the normal contact pressure distribution in the contact area is given by the Hertz theory:

$$p(r) = p_0\sqrt{1-\left(\frac{r}{a}\right)^2} \tag{2}$$

where a is the contact radius, $p_0 = (6PE^{*2}/\pi^3R^2)^{1/3}$ is the maximum contact pressure and E^* is the reduced modulus [20]. The

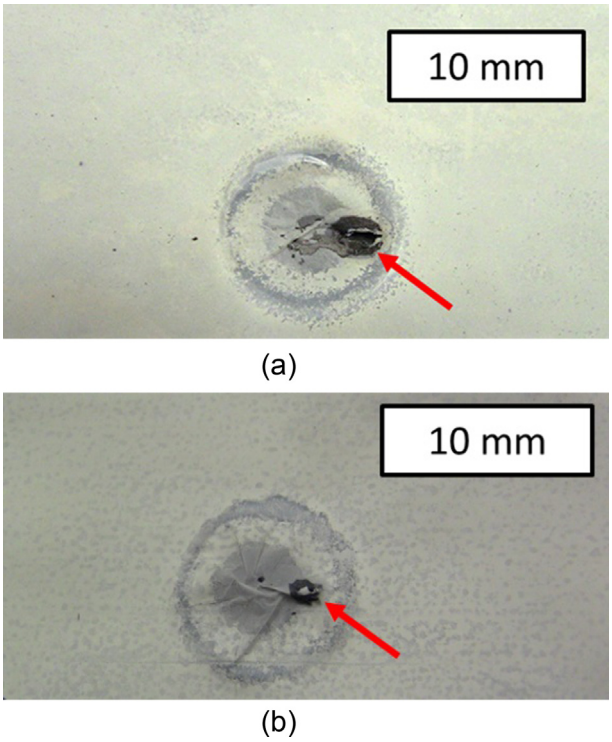

Fig. 5. Optical graphs showing broken separators after (a) a pinch test and (b) a pinch–torsion test. The pointed cracks in the separator layer are initiated outside the spherical contact surface for both tests.

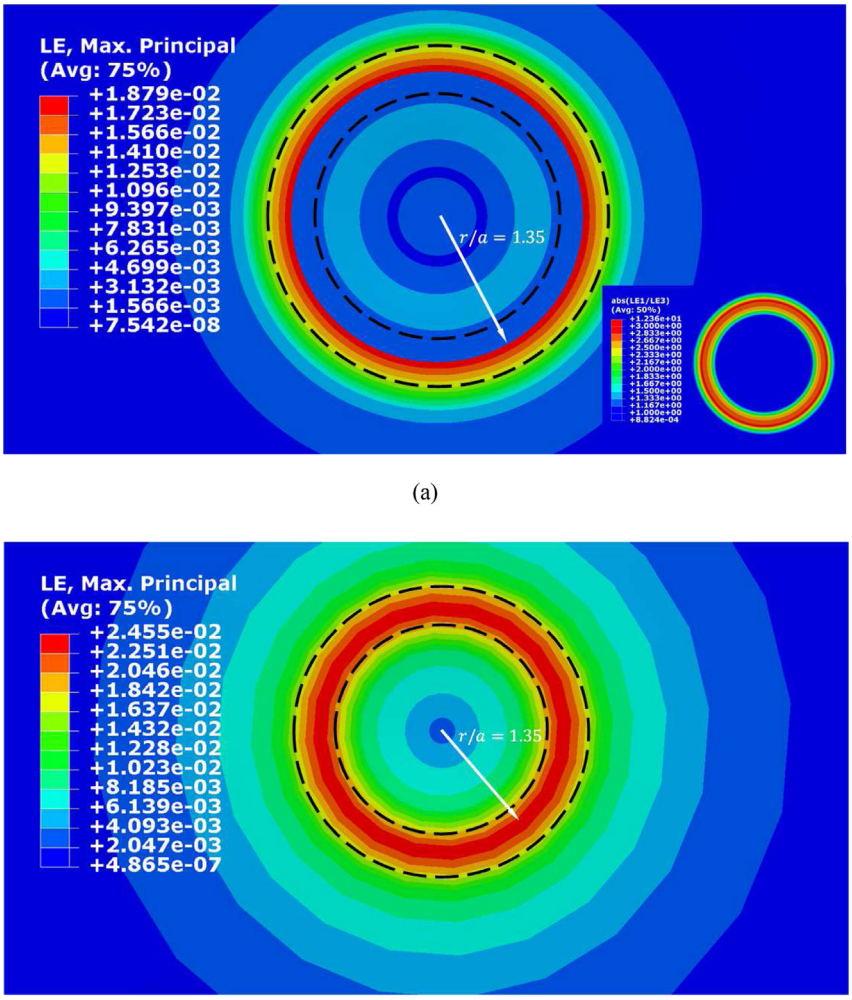

Fig. 6. Simulated distribution of ε_1 in separator layer (a) before twisting (b) after twisting with angle of 12°. The black dash lines denote the tension zone.

maximum contact pressure resides on the center of the contact area and monotonically decreases along the radial direction. If a torque M_z is applied, the tangential traction $q(r)$ in the contact area is distributed as,

$$q(r) = \frac{3M_z r}{4\pi a^3}\left(a^2 - r^2\right)^{-0.5} \tag{3}$$

where, mathematically, the torsional shear traction goes to infinity at the edge of the contact area (i.e. $r \to a$). Such a solution is similar to the Mode-III crack tip field at the contact edge where the classic inverse-square-root singularity resides, and obviously it holds only when the interface is perfectly bonded. According to the Coulomb friction law, when $|q(r)| \le \mu|p(r)|$, there is no tangential slip between the two contact surfaces, and when $|q(r)| > \mu|p(r)|$, there will be a relative slip between the indenter and the substrate. The shear stress singularity at the contact edge clearly leads to the stick-slip behavior as shown in Fig. 8a. From Eq. (3), after a torque $M_z(\theta)$ is applied, where θ is the twist angle, the edge of the contact surface will start to slip immediately due to the large tangential traction. However, the rest of the region in the contact area remains bonded, making the indenter contact surface partially slip on the solid. For any point in the contact area which has a distance r to the contact

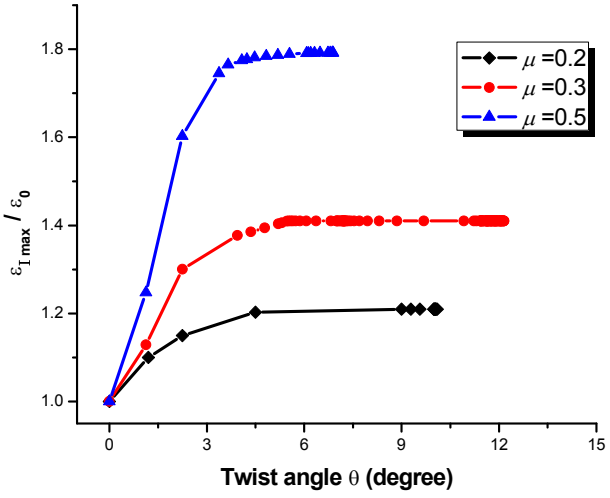

Fig. 7. The maximum first principal strain ε_1 as a function of twist angle θ with different friction coefficients μ. The strain ε_1 during the torsion test is normalized by the maximum first principal strain in HDPE when the pinch test ends which has negligible dependence on the friction coefficient.

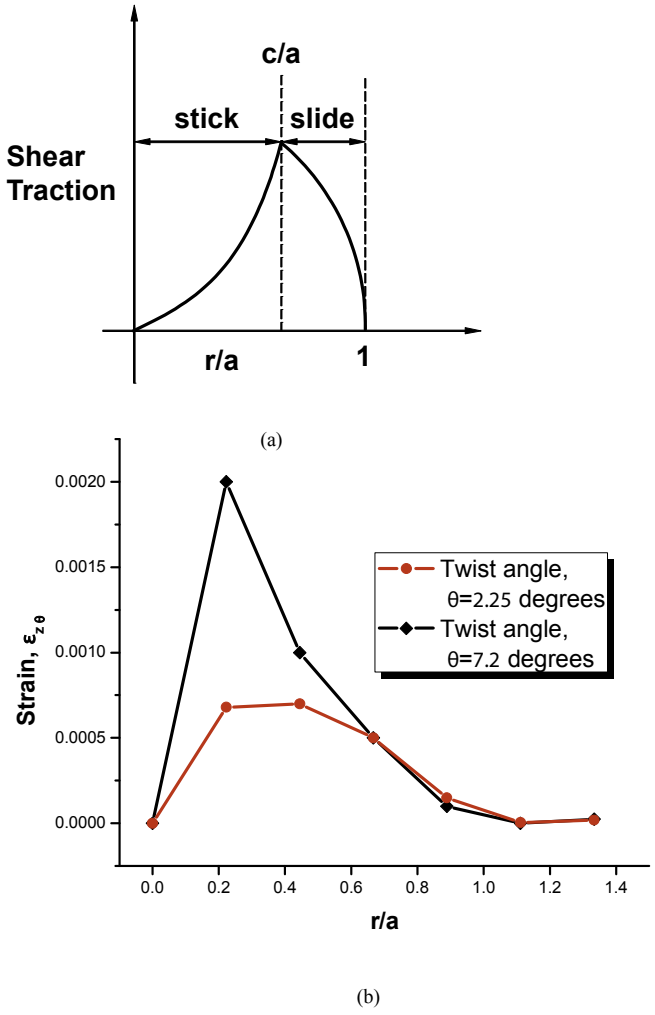

Fig. 8. (a) Shear traction $q(r/a)$ distribution when the indenter is under partial slip. (b) The strain $\varepsilon_{z\theta}$ distribution along the radius at the contact surface when $\theta = 2.25^\circ$ and 7.2°.

center, the critical twist angle needed to initiate the slide is related to indent pressure as,

$$q(r) = \mu p(r) = \frac{3\mu P}{2\pi a^3}\left(a^2 - r^2\right)^{\frac{1}{2}} \tag{4}$$

In this study, we assume the static friction coefficient is the same as the kinetic friction coefficient. Therefore, once the two contact surfaces change state from stick to slip, the tangential traction will remain as a constant at the value of maximum static shear force, i.e. $\mu p(r)$. The largest $q(r)$ and thus the largest shear stress $\tau_{z\theta}$ in the contact surface always occurs at the place where it is just start to slip. We denote the distance between the $q(r)$ maxima and the contact center as $c(\theta)$. A representative profile of $q(r/a)$ when the indenter partially slips on the contact surface is plotted in Fig. 8a. Where $q(r)$ reaches its peak at $c(\theta)$. For location $r > c(\theta)$ in the contact area, it is in dynamic slipping while location remains static at $r < c(\theta)$. The shear stress $\tau_{z\theta}$ will add a large shear strain $\gamma_{z\theta}$ and thus increase the maximum ε_I, corresponding the ascending part in Fig. 4. The stick circle eventually shrinks towards the contact center (i.e. $c(\theta) \to 0$) and the free sliding of the indenter is started with a constant moment M_z. Therefore, no further deformation takes place in the battery system and the maximum first principal strain ε_1 arrives in the plateau shown in Fig. 7.

The above analytic solution is derived from elastic half-spaces. For the thin layer under a pair of spherical contacts, the stick-slip behavior applies qualitatively, but its quantitative feature can only be obtained from finite element analysis. The strain $\varepsilon_{z\theta}$ is plotted along the radius at the battery contact surface with twist angles: 2.25° and 7.2° respectively in Fig. 8b. For $\theta = 2.25$, the maximum shear strain appears at $c(\theta) = 0.3a$. For $\theta = 7.2^\circ$, the indenter has fully slipped so that max $\varepsilon_{z\theta}$ appears in the vicinity of contact. Based on the analysis above, it is confirmed that torsion of the indenter will increase the intensity of tension inside the sample thus will increase the possibility of breaking the separator layer. However, such effect saturates beyond a critical twist angle and ε_1 remains relatively constant, which depends on the friction coefficient μ.

To explore ε_1 plateau value in the separator layer, the influence of friction coefficient μ between the surfaces is presented in Fig. 9. It shows that the plateau monotonically increases with the increase of friction coefficient μ because from Eq. (3), larger friction coefficient will lead to larger tangential stress and thus larger principal tensile strain. In other words, when μ is large, a larger torque is needed to produce a specific twist angle for the indenter, and thus the separator layer will have more severe deformation to assist the defect initiation. In conclusion, torsion component facilitates the failure of the sample by increasing tensile deformation in the polymeric separator.

Our recent study compared the pinch and pinch–torsion tests in terms of the axial load needed to induce ISCr [11]. For a three-layer dry cell that had a configuration similar to Fig. 2, it was discovered the axial load generating ISCr decreased from approximately 630 N under pure pinch loading to about 400 N under a combined pinch/torsion loading – a reduction of 36.5% [11]. The reduction is explained in Fig. 10 where a fix twist angle is applied to different indenter force F and the maximum principle strains in different cases are plotted. We also make a pinch-only test, as a reference case, by applying an indentation force F_0 on the unit cell and read the maximum first principle strain ε_0 without any twist to the indenter. Fig. 10 shows that after a slight twist angle 2.7° is applied, one would need less indentation force (a reduction of 33%) to create same amount of maximum first principal strain (i.e. $\varepsilon_1/\varepsilon_0 = 1$) in the unit cell. It is in line with what is observed in our recent study [11]. On the other hand, it is noticed that at the same applied load, the

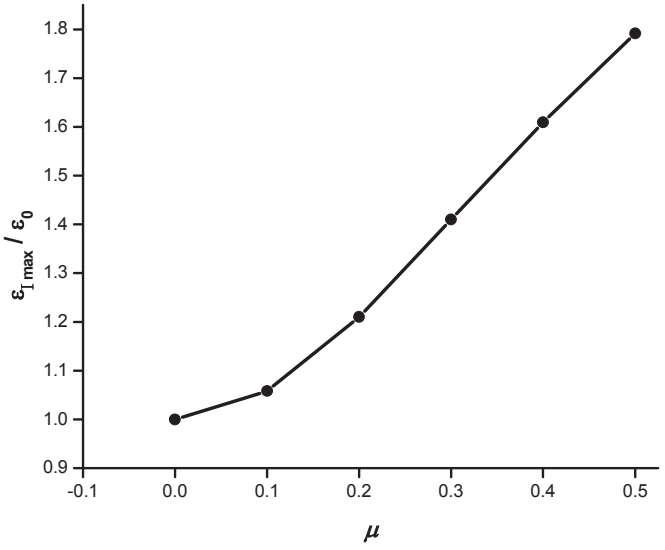

Fig. 9. The maximum first principal strain ε_1 after the indenter is twisted with an angle $\theta = 6$ as a function of friction coefficients μ.

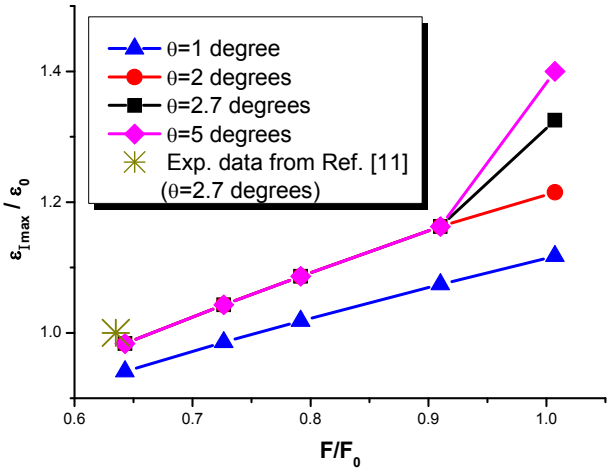

Fig. 10. The maximum first principal strain ε_1 as a function of indentation force at different fixed twist angles. F_0 and ε_0, respectively, are the indentation force and the maximum first principal strain when no twisting is applied. The experimental data point was taken from Ref [11], which represented results from multiple measurements. Since those samples were nominally identical they failed under similar conditions and appeared to be a "single" data point in Fig. 10, which has normalized axes.

maximum first principle strain inside HDPE increases significantly with θ from 1° to 2°. The coincidence of data for angles larger than 2° shows that the indenter is in dynamic slipping already after twisted 2° at small applied load level (i.e. F/F_0 is less than 0.9). When indenting with a large load, e.g. $F/F_0 \rightarrow 1$, higher twisting angle is needed to make the contacting surfaces fully slip. And the maximum first principle strain increases by 17% with the twisting angle θ from 2° to 5°.

4. Conclusions

In this paper, finite element analysis is used to simulate deformation of Li-ion battery layers under pinch and pinch–torsion conditions. The simulation discovery is in agreement with our previous experimental results. Several conclusions can be drawn as follows:

1. Spherical indentation delivers tensile zone inside the sample instead on the surface comparing with other experiments such as flat end punch and bending test, making it an attractive method to simulate ISCr in Li-ion batteries.
2. A slight twist of the indenter introduces the shear strain, which increases the maximum first principal strain in tension zone and thus facilitates the failure of the polymer. During this stage, the indenter and the contact surface partially slip with co-existence of a slip region and a stick region.
3. Beyond a critical angle, the indenter is free to spin relative to the battery and the maximum first principal strain ε_1 takes its limit value, which highly depends on the friction coefficient μ. Therefore, controlling surface condition on the indenter or battery surface could be utilized to control ISCr events.

Acknowledgment

This work was sponsored by the Office of Vehicle Technologies of the Department of Energy and was carried out at Oak Ridge National Laboratory under contract DE-AC05-00OR22725 with UT-Battelle, LLC. The authors acknowledge the support from NSF CMMI 0900027 (YZX), and the U.S. Department of Energy, Basic Energy Sciences, Materials Sciences and Engineering Division (YFG). FR would like to thank the College of Engineering at Temple University for its financial support during manuscript preparation. TLT would like to acknowledge the support in part by the State of Florida and the National Science Foundation through NSF Cooperative Grant DMR 0654118.

References

[1] D. Belov, M.H. Yang, J. Solid State Electrochem. 12 (2008) 885–894.
[2] H. Maleki, J.N. Howard, J. Power Sources 191 (2009) 568–574.
[3] R. Spotnitz, J. Franklin, J. Power Sources 113 (2003) 81–100.
[4] M.L. Lee, Y.H. Li, J.W. Yeh, H.C. Shih, J. Power Sources 214 (2012) 251–257.
[5] Battery Association of Japan, Presentation at UN Informal Working Group Meeting, November 11–13, 2008. Washington, DC.
[6] Underwriters Laboratories Inc., Presentation at UN Informal Working Group Meeting, November 11–13, 2008. Washington, DC.
[7] L. Florence, Presentation at Battery Power, 2010. Dallas, Texas.
[8] J.P. Peres, F. Perton, C. Audry, et al., J. Power Sources 97–98 (2001) 702–710.
[9] W. Cai, H. Wang, H. Maleki, et al., J. Power Sources 196 (2011) 7779–7783.
[10] E. Sahraei, R. Hill, T. Wierzbicki, J. Power Sources 201 (2012) 307–321.
[11] F. Ren, T. Cox, H. Wang, J. Power Sources 249 (2014) 156–162.
[12] K.H. Shim, S.H. Lee, B.S. Kang, S.M. Hwang, J. Mater. Process. Technol. 155 (2004) 1935–1942.
[13] A.F. Bower, CRC Press, Boca Raton, 2009.
[14] D.J. Hughes, A. Mahendrasingam, W.B. Oatway, et al., Polymer 38 (1997) 6427–6430.
[15] N.O. Cardenas, I.F. Machado, E. Goncalves, J. Mater. Sci. 42 (2007) 6935–6941.
[16] Y. Ide, J. White, J. Appl. Polym. Sci. 22 (1978) 1061–1079.
[17] K.L. Johnson, Cambridge University Press, Cambridge, 1985.
[18] E. Dintwa, M. Van Zeebroeck, E. Tijskens, H. Ramon, Eur. Phys. J. B 39 (2004) 77–85.
[19] T. Li, J.H. Lee, Y.F. Gao, Int. J. Appl. Mech. 1 (2009) 515–525.
[20] T. Li, Y.F. Gao, H. Bei, E.P. George, J. Mech. Phys. Solids (2011) 1147–1162.